

# PFD: Automatically Generating Machine Learning Force Fields from Universal Models

Ruoyu Wang<sup>1,2</sup>, Yuxiang Gao<sup>1,2</sup>, Hongyu Wu<sup>3</sup>, and Zhicheng Zhong<sup>1,2,3\*</sup>

<sup>1</sup>*School of Artificial Intelligence and Data Science,*

*University of Science and Technology of China, Hefei 230026, China*

<sup>2</sup>*Suzhou Institute for Advanced Research, University of Science and Technology of China, Suzhou 215123, China and*

<sup>3</sup>*Suzhou Lab, Suzhou 215123, China*

Universal force fields generalizable across the periodic table represent a new trend in computational materials science. However, the applications of universal force fields in material simulations are limited by their slow inference speed and the lack of first-principles accuracy. Instead of building a single model simultaneously satisfying these characteristics, a strategy that quickly generates material-specific models from the universal model may be more feasible. Here, we propose a new workflow pattern, PFD, which automatically generates machine-learning force fields for specific materials from a pre-trained universal model through fine-tuning and distillation. By fine-tuning the pre-trained model, our PFD workflow generates force fields with first-principles accuracy while requiring one to two orders of magnitude less training data compared to traditional methods. The inference speed of the generated force field is further improved through distillation, meeting the requirements of large-scale molecular simulations. Comprehensive testing across diverse materials including complex systems such as amorphous carbon, interface, *etc.*, reveals marked enhancements in training efficiency, which suggests the PFD workflow a practical and reliable approach for force field generation in computational material sciences.

## I. INTRODUCTION

First-principles density functional theory (DFT) method enables highly accurate material simulations by providing precise predictions of energy and forces in arbitrary atomistic systems. Yet its application is generally limited to systems with only a few hundred atoms due to the exponential scaling in computational cost with system size. Recently, machine learning force fields trained on first-principles data, *e.g.*, DeePMD[1], GAP[2], *etc.*, have emerged as a promising alternative, effectively addressing the limitations in size- and time-scales while maintaining DFT-level accuracy[2–7]. However, training machine learning force fields remains a complex and resource-intensive task. Constrained by primitive model architecture and parameterization, many machine learning force fields exhibit poor generalization and cover only narrow chemistry[8]. Consequently, data generation and model training must be carried out for each specific system from scratch. Moreover, the training procedure is inefficient, often requiring thousands of costly first-principles calculations and advanced techniques such as concurrent learning and iterative refinement, even for simple crystals[9]. For complex realistic systems, such as surfaces, interfaces, heavily doped materials, and amorphous materials, the training process becomes extremely difficult and prohibitively expensive, making it challenging to achieve practical applicability[10, 11].

In recent years, there has been significant development in universal force fields with broad coverage, as amplified by models such as DPA-2[12], MatterSim[13],

ORB[14], MACE[15, 16] and M3GNet[17], among others[17–22]. With their sophisticated model architecture, universal force fields exhibit exceptional generalizability after training using millions of first-principles calculations covering a wide range of materials. Ideally, universal force fields are applicable to any materials without the need for additional training and have seemingly addressed the issues of the more "traditional" machine learning force fields. Nevertheless, universal force fields still face key challenges despite being highly generalizable. Firstly, the energy error of universal force fields is usually in the range of a few dozens meV per atom; this may be insufficient for material simulation requiring first-principles accuracy (energy error within a few meV per atom). Another challenge for universal force fields is the much higher computational cost due to the complex model architecture[22, 23]. Because of these problems, universal force fields are not suitable for accurate large-scale material simulation, which usually requires tens of thousands of atoms. Great efforts have been made to develop universal force fields that are simultaneously generalizable, accurate, and efficient, but achieving this goal remains challenging due to the conflicting nature of these requirements (Table I). Therefore, rather than building a single perfect model, a more practical strategy could be to generate fast, material-specific force fields from a universal force field with prior knowledge[12, 13].

Here, we propose a workflow pattern named **PFD**, designed to automatically generate material-specific machine learning force fields from a pre-trained universal model (**P**) through fine-tuning (**F**) and distillation (**D**). In the fine-tuning stage, the pre-trained foundation model is retrained on a small dataset of DFT calculations to produce a highly accurate, material-specific model. In the following distillation stage, the fine-tuned model is

\* zczhong@ustc.edu.cn

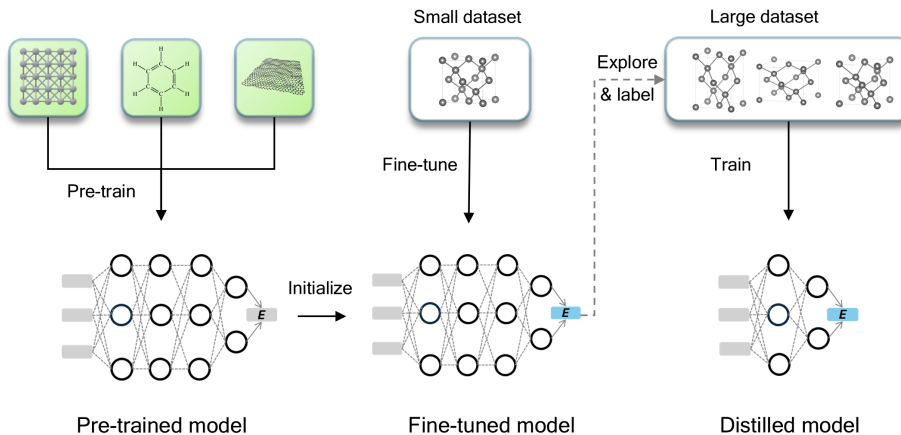


Figure 1. **Schematic of the PFD workflow concept.** A material-specific model with first-principles accuracy is trained by fine-tuning a pre-trained universal model using a small set of first-principles calculations. For improved simulation speed, a simplified model is trained using the dataset generated and labeled by the fine-tuned model.

employed to label a large dataset of energies and forces, which is then used to train a simplified model. This distilled model retains first-principles accuracy while being computationally efficient for specific materials. Extensive tests of the PFD workflow on a wide range of materials demonstrate remarkable performance. Compared to traditional training methods, the PFD workflow reduces the required first-principles calculations by 1 to 2 orders of magnitude, significantly saving both time and computational resources. Moreover, the PFD workflow enables the construction of practical force fields for complex materials, such as amorphous phases and material interfaces, which are otherwise extremely difficult. These promising results suggest that the PFD workflow is a practical and efficient approach to machine learning force field generation in computational material science.

## II. METHODOLOGY

The underlying principle of the PFD workflow is shown in Figure 1. At the core of the PFD concept is the universal force field, also known as the large atomic model, which is pre-trained across a large chemical space that may include crystal materials, molecules, and more. Major candidates for the large atomic model include DPA-2[12], MACE[16], MatterSim[13], GNoME[24], *etc.* In this work, we utilize the public version of the DPA-2 pre-trained model[25] as the foundation model. A key feature of the DPA-2 model is its diverse training datasets, which include general datasets like MPTrj, as well as domain-specific datasets for ferroelectric materials, drugs, alloys, *etc.* By an advanced multi-task pre-training process, knowledge from vastly different datasets with their distinct DFT labels is fused into a single, unified descriptor shared across multiple prediction heads. This feature makes the pre-trained DPA-2 an ideal candidate for the

foundation model of our PFD workflow.

By fine-tuning the foundation model, a highly accurate, material-specific model can be trained using a small DFT training dataset. Figure 2 illustrates the iterative fine-tuning strategy adopted by the PFD workflow. Initially, a small dataset is created by randomly perturbing the structures of the input material and labeling them through DFT calculations. The initial dataset is used to refine the pre-trained model. Then, MD simulations driven by the fine-tuned model are conducted to explore new configurations, which are then labeled with DFT calculations. If the fine-tuned model fails to accurately predict the labeled dataset, the labeled data are selectively added to the training set for the next iteration. This exploration, labeling, and fine-tuning process is iterated until the convergence criterion is achieved. To avoid excessive sampling of equilibrium configurations, a labeled data point would be filtered out if its energy or force prediction error is below a certain threshold. Similarly, a labeled data point with large prediction errors is also excluded to ensure the stability of the training process. Another potential issue in this iterative process is the potential accumulation of training data across iterations. Therefore, in each iteration, the model can be reinitialized using the fine-tuned model from the previous iteration based on the user’s decision and fine-tuned using a mix of new and old training datasets in a predetermined ratio.

Once the iterative fine-tuning has been completed, the PFD workflow can move to the distillation phase. In this phase, the fine-tuned model directly generates a large dataset of new configurations by MD simulations. The energy and force of the new configurations are labeled using the fine-tuned model, which is almost free compared to the expensive DFT calculations, as shown in Figure 2. Then a simpler and faster force field for specific materials is trained using this large dataset following stan-

Table I. General characteristics of typical force fields for atomistic simulation. The efficiency includes both the capability for MD simulations and the DFT calculations required for training. The simulation capability is measured by system size and the time consumed for a single step in MD simulation.

	DFT (VASP, ABACUS, <i>etc.</i> )	Classical MLFF (DeepMD, GAP <i>etc.</i> )	Universal MLFF (DPA-2, MACE, M3GNet, <i>etc.</i> )	PFDF
Generalizability	any material	specific materials	most of materials	any material after fine-tuning
Accuracy	—	< 5 meV/atom	< 50 meV/atom	< 5 meV/atom
Efficiency*	500 atoms, $10^4$ s; —	100,000 atoms, 0.5 s; 2000 DFT calc.	2,000 atoms, 0.5 s; —	100,000 atoms, 0.5 s; 100 DFT calc.

\* Estimated for typical inorganic crystals. See Supplementary Information for specific hardware specification.

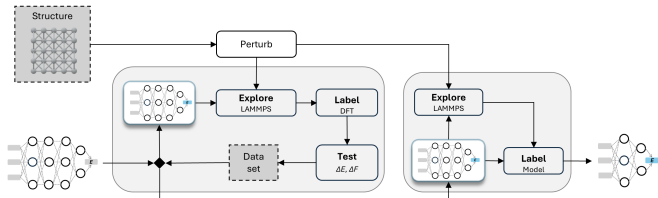


Figure 2. **Iterative scheme of PFD workflow.** PFD workflow consists of two phases. In the fine-tuning phase, PFD explores new structures with the fine-tuned model and label them with first-principles calculation, then a new model is trained with the updated training set. This process would iterate until convergence is achieved. In the distillation phase, the fine-tuned model would be used to explore and label a large dataset, which would be used to train a distilled model in a single run.

standard training procedures. In this work, all distilled force fields are standard DeepMD models using local descriptors. Unlike fine-tuning, the distillation is completed in a single iteration since exploration with the fine-tuned teacher model is highly stable. To implement the PFD workflow, we have developed a Python package named PFD-kit, which utilized the dflow workflow package design for scientific calculations[26]. A more detailed description of the technical aspect of the PFD-kit can be found in the Supplementary Information.

### III. RESULTS

#### A. Data efficiency of fine-tuning

The foundation of PFD lies in the significant reduction in DFT first-principles calculations by fine-tuning a pre-trained universal model. Figure 3 illustrates the data efficiency of fine-tuning in comparison with training from scratch. Here, a dataset of solid electrolyte materials  $\text{Li}_6\text{PSCl}_5$ [27] was collected using the DPGEN active learning scheme[28], which consisted of nearly 4000 energy data points. The dataset was randomly partitioned into small training sets of various sizes, which were then used to train a force field either from the pre-

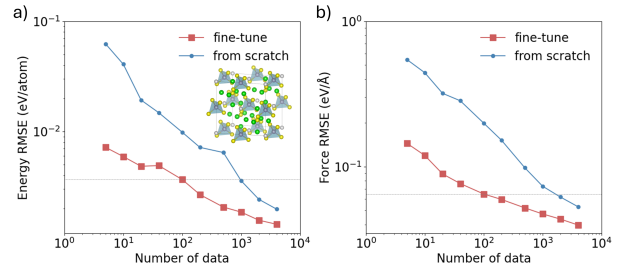


Figure 3. **Data efficiency of fine-tuning.** The figure illustrates the fine-tuning performance of a pre-trained DPA-2 model using subsets of the argyrodite  $\text{Li}_6\text{PS}_5\text{Cl}$  solid electrolyte of various sizes. It highlights the convergence of energy and atomic force prediction accuracy with dataset sizes. The crystal structure of  $\text{Li}_6\text{PS}_5\text{Cl}$  is also presented.

trained model or from a randomly initialized model of the same network structure. The pre-trained model fine-tuned with 100 first-principles data points was more accurate than the random model trained from scratch with 1000 data points, as indicated by the dotted line in Figure 3, by utilizing the transferable knowledge in the pre-trained model. This reduction in the training dataset not only saves large computational resources used for expensive first-principles calculations, but also accelerates the structure exploration and training processes. For example, the fine-tuning phase of PFD typically converges within only a few iterations, contrary to traditional active learning methods which need to collect a large number of configurations in many more iterations. As a result, the throughput of model generation is also significantly improved, with a much shorter waiting time and more robust workflow control when using the PFD workflow.

#### B. Bulk Materials

As an example, we present the results for crystalline silicon, a fundamental semiconductor. In the fine-tuning phase, PFD selected 66 frames from MD trajectories at 1000 K under pressures of up to 1 GPa and labeled them with DFT calculations. Among the DFT dataset, 33 data points were added to the training dataset, while the rest

served as the test dataset. The energy and force root mean square error (RMSE) of the fine-tuned model are 0.0019 eV and 0.0389 eV/Å, respectively, as illustrated in Figures 4a and 4b. In the distillation phase, the fine-tuned model explored and labeled a large dataset containing 1500 energy data points by running MD simulations at 1000 K under pressures up to 1 GPa. The distilled model was then trained using 1,350 of these labeled data points, following the standard one-time training procedure for the DeePMD model. The energy and force RMSE of the distilled model are 0.0021 eV and 0.0556 eV/Å, as shown in Figures 4c and 4d, respectively. The inset of Figure 4 compares the efficiency of the fine-tuned and distilled models. Due to its much simpler model architecture, the inference speed of the distilled model is almost two orders of magnitude faster. Table II lists the training cost and accuracy of the crystalline silicon models generated using the PFD workflow. For bulk materials such as crystalline silicon, the PFD workflow enables a fully automatic generation of force fields with first-principles accuracy at minimal cost in a few hours.

Table II. Training cost and accuracy of the fine-tuned and distilled models for crystalline silicon generated using the PFD workflow

	Fine-tuning	Distillation
Data size	33	1350
Number of iterations	2	1
Time <sup>a</sup>	1.5 h	1.5 h
Energy RMSE (eV/atom)	0.0019	0.0021

<sup>a</sup> See Supplementary Information for hardware specifications.

Training force fields for crystalline silicon is relatively straightforward due to its simple structure and narrow chemical space. To evaluate the performance of the PFD workflow in a more complex scenario, where the bulk material exhibits moderate doping or element mixing, we applied it to a NASICON (sodium superionic conductor)-structured solid electrolyte  $\text{Li}_{1+x}\text{Al}_x\text{Ti}_{2-x}(\text{PO}_4)_3$ [29]. Starting from the pre-trained model, new configurations were generated from 700 K MD trajectories under pressures up to 1 GPa. In three iterations, 215 frames were collected for DFT calculation, of which 138 frames were selected for fine-tuning. The resulting fine-tuned model exhibits high accuracy, with energy and force RMSE of 0.0013 eV/atom and 0.0510 eV/Å, respectively (Figure 5). Accurate lithium-ion transport simulations at room temperature require long MD trajectories with a large simulation cell to achieve sufficient equilibrium and mitigate finite-size effects[30, 31]. To this end, a simple yet highly efficient DeePMD model for  $\text{Li}_{1+x}\text{Al}_x\text{Ti}_{2-x}(\text{PO}_4)_3$  was generated by distillation for fast atomistic simulations. During the distillation process, 2727 frames were generated and labeled using the fine-tuned model, and 2455 of them were used to train the DeePMD model. The training set includes  $\text{Li}_{1+x}\text{Al}_x\text{Ti}_{2-x}(\text{PO}_4)_3$  structures of four different com-

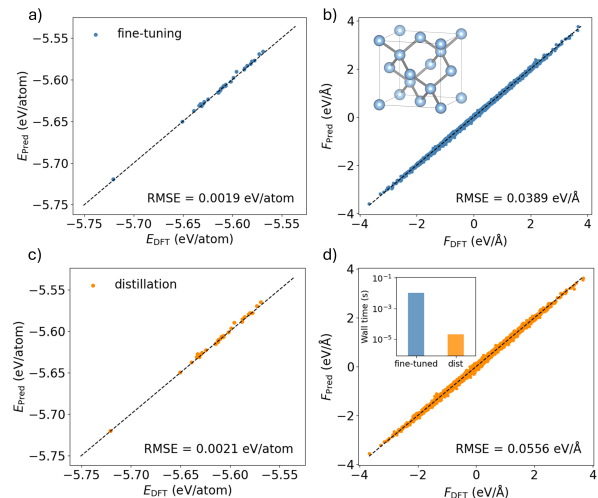


Figure 4. **Force field for crystalline silicon generated from PFD workflow.** The accuracy of the fine-tuned model for **a)** energy and **b)** atomic force prediction. The **c)** energy and the **d)** force prediction error of the distilled model. The test set is extracted from MD trajectories at 1000 K and under various pressures up to 1 GPa. The inset of **d)** compares the efficiency of the fine-tuned and distilled models in terms of CPU wall time for each atom per time step.

positions, *i.e.*,  $x = 0.16, 0.32$  and  $0.5$ . Figure S3 shows the accuracy of the distilled model, which is then used to simulate lithium-ion transport in  $\text{Li}_{1.3}\text{Al}_{0.3}\text{Ti}_{1.7}(\text{PO}_4)_3$  ( $x = 0.3$ ) using a large simulation cell of 3520 atoms. Figure 5c shows the calculated temperature-dependent diffusion coefficient of lithium ions from 300 K to 900 K. For comparison, previous ab initio molecular dynamics (AIMD) results using a small cell of 110 atoms are also listed here[32]. At high temperatures, the diffusion coefficient from the distilled model converges with that from the AIMD simulation, as the insufficient sampling due to small cells and short trajectories becomes negligible. However, accurate room temperature simulations of lithium-ion transport are beyond the reach of AIMD method due to the substantial computational cost. Using the Arrhenius law, the activation energy for lithium-ion hopping in  $\text{Li}_{1.3}\text{Al}_{0.3}\text{Ti}_{1.7}(\text{PO}_4)_3$  was estimated to be 0.18 eV, consistent with the experimental measurement. This result highlights the potential of the PFD workflow in generating highly accurate and efficient force fields for accurately *predicting* key dynamic properties such as ionic conductivity. Beyond this, PFD offers opportunities for complex materials simulations that were previously inaccessible, enabling high-throughput studies of structural dynamics, transport phenomena and other critical properties across diverse material systems.

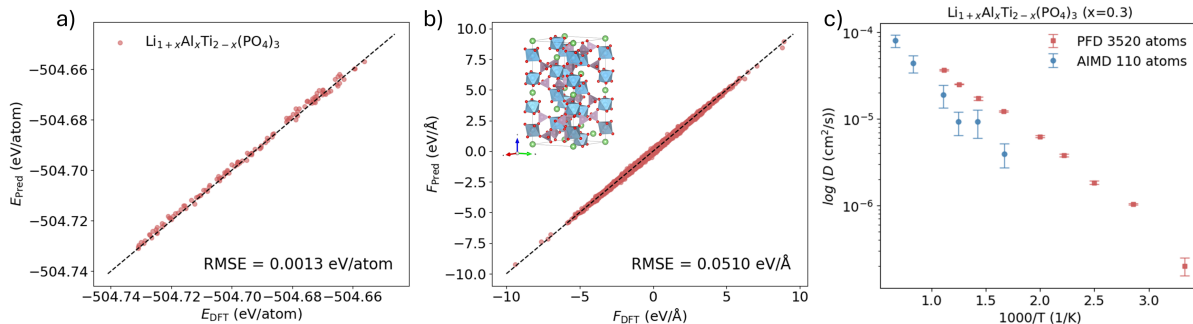


Figure 5. **Ion transport in  $\text{Li}_{1+x}\text{Al}_x\text{Ti}_{2-x}(\text{PO}_4)_3$  solid electrolyte.** The **a)** energy and the **b)** force prediction error of the distilled model for  $\text{Li}_{1+x}\text{Al}_x\text{Ti}_{2-x}(\text{PO}_4)_3$  solid electrolyte. **c)** The temperature-dependent diffusion coefficients  $D$  of  $\text{Li}_{1.3}\text{Al}_{0.3}\text{Ti}_{1.7}(\text{PO}_4)_3$  calculated using the distilled model. For comparison, high-temperature  $D$  calculated using AIMD simulations in a small cell from a previous study[32] are also listed here. The interpolated activation energy barrier is 0.18 eV.

### C. Complex Materials

In the previous section, we have demonstrated that the PFD workflow can automatically generate force fields capable of large-scale MD simulation with first-principles accuracy for bulk materials. However, training force fields for complex materials presents further challenges as the exponential increase in possible element combinations and spatial configurations. Consequently, the number of first-principles calculations required to train such force fields becomes intractable. Fortunately, the PFD workflow can circumvent this issue by leveraging the pre-trained foundation model and reducing the required first-principles calculations to an acceptable level. In this section, we extend the application of the PFD workflow to four examples of complex materials that encompass molecules, amorphous materials, and interfaces, showcasing its versatility and efficiency in tackling diverse and intricate material systems.

Compared with inorganic crystals, molecular systems present new challenges for atomistic simulation due to their complex intermolecular interactions (hydrogen bond, van der Waals force, *etc.*) and conformational flexibility. As a result, training machine learning force fields for molecular systems typically requires a large quantity of data to capture their statistical and dynamical properties. Fine-tuning from a pre-trained universal model using the PFD workflow can greatly reduce the cost of model training and data generation. Here, we trained a model for 1,4-polyisoprene molecular chains by PFD workflow. Figure 6 shows the typical conformation of a group of eight molecular chains of 1,4-polyisoprene, and the inset image is a single chain consisting of multiple 1,4-polyisoprene building blocks. Within two fine-tuning iterations, 157 DFT calculations of single polyisoprene chains were collected and used to train the model. The fine-tuned model was tested on a dataset of molecular chain clusters. The energy and force RMSE were 0.0027 eV/atom and 0.0562 eV/Å, respectively. It is worth noting that intermolecular van der Waals forces, which are

absent in the single-chain training dataset, influence the energy of molecular chain clusters. Hence, there is an observed energy shift of 0.0026 eV/atom, as indicated by the thin dotted line in Figure 6. After accounting for this energy shift, the energy RMSE then decreases to 0.0005 eV/atom.

The second example is amorphous carbon with a large amount of possible spatial configurations. Traditionally, thousands of first-principles DFT calculations are required to exhaust the configurations and train viable force fields, which can be extremely expensive[33]. To verify the effectiveness of the PFD workflow for amorphous materials, a large set of amorphous carbon with  $sp^3$  hybridization was randomly generated[34]. The fine-tuning set was initialized with a small subset of the generated structures and extended by MD explorations at 500 K. In total, 655 out of 1022 DFT calculations were selected for fine-tuning. Figure S5 shows the accuracy of the fine-tuned model on configurations from the training set, with the energy and force RMSE of 0.0059 eV/atom and 0.0661 eV/Å, respectively. An important application of such a force field is the prediction of new amorphous structures that were not explicitly included in the training set. Thus, the fine-tuned model was tested on a dataset consisting of new  $sp^3$  amorphous carbon not present in the training dataset. As shown in Figure 7, the fine-tuned model accurately predicted these unseen  $sp^3$  carbon structures with an energy RMSE of 0.0054 eV/atom. This result demonstrates the potential of the PFD workflow when integrated with structure generation algorithms to efficiently search for metastable amorphous configurations.

The third example involves a high entropy perovskite structure,  $\text{Ba}_{0.5}\text{Na}_{0.25}\text{Bi}_{0.25}\text{Ti}_{0.875}\text{Zr}_{0.125}\text{O}_3$ , featuring multiple doping elements. Training an accurate force field for such systems is challenging due to the large number of possible local combinations of elemental atoms, which usually requires thousands of DFT calculations even with active learning algorithms[35, 36]. Using the PFD workflow, this challenge is effectively addressed. A

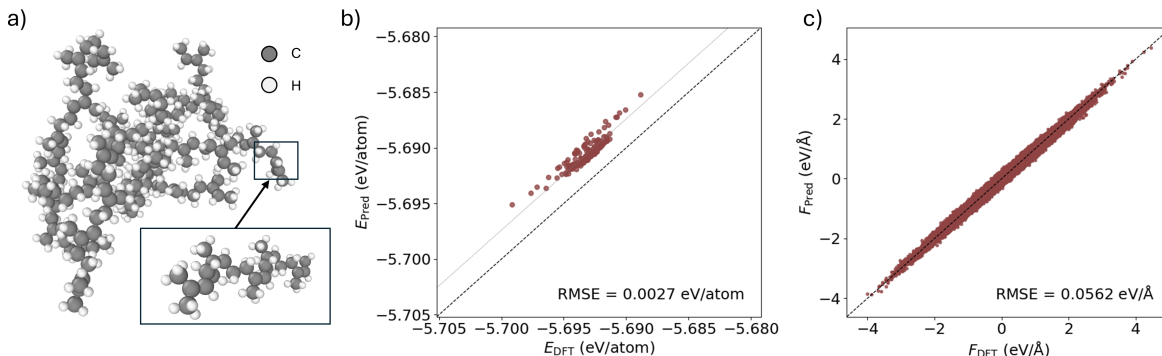


Figure 6. **Fine-tuned model for polyisoprene chain.** **a)** A cluster of several polyisoprene chains. The inset image is one single polyisoprene chain which consists of several 1,4-polyisoprene building blocks. The **b)** energy and the **c)** force prediction accuracy of the fine-tuned model generated using the PFD workflow. Note that the thin dotted line in **b)** indicates the overall energy shift possibly due to intermolecular interactions between polyisoprene chains.

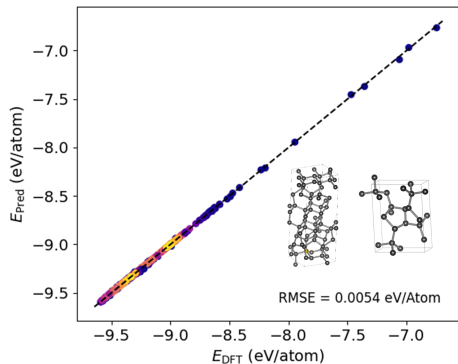


Figure 7. **Predicting new amorphous carbon structures using fine-tuned model generated by the PFD workflow.** The fine-tuned model is trained on a small portion of amorphous carbon with  $sp^3$  hybridization, and it can accurately predict  $sp^3$  amorphous carbon not present in the training set. The energy RMSE is 0.0054 eV/atom. The inset picture shows unit cells of two  $sp^3$  amorphous carbons.

small training set is constructed from MD trajectories at 500 K under atmospheric pressure, which includes only 134 DFT calculations. The fine-tuned model exhibits high accuracy, with an energy RMSE of 0.0010 eV/atom and a force RMSE of 0.0472 eV/Å, respectively. In the distillation phase, 3818 labeled configurations were generated with the fine-tuned model and then used to train a distilled model. The distilled model achieved an energy RMSE of 0.0014 eV/atom and a force RMSE of 0.0691 eV/Å, respectively, as shown in Figure 8. The significant contrast in the amount of training data required for fine-tuning versus distillation suggests that the PFD workflow reduces the DFT calculations by more than an order of magnitude compared to traditional methods.

The last example focuses on the interface between  $\text{Li}_6\text{PSCl}_5$  solid electrolyte and lithium metal

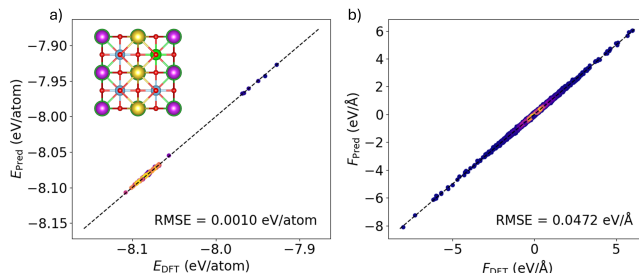
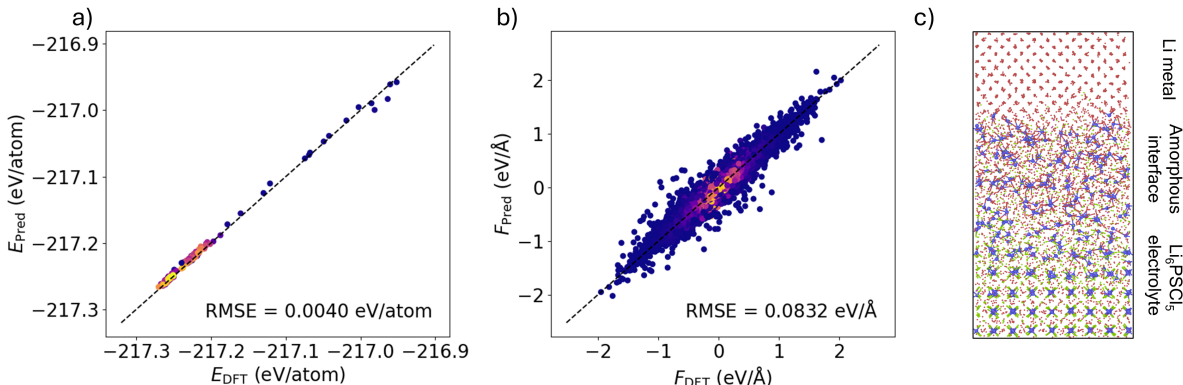


Figure 8. **The model of perovskite  $\text{Ba}_{0.5}\text{Na}_{0.25}\text{Bi}_{0.25}\text{Ti}_{0.875}\text{Zr}_{0.125}\text{O}_3$  generated using PFD workflow.** The **a)** energy and the **b)** force prediction error of the fine-tuned model. Points with brighter color corresponds to higher density.

electrode[37]. Although extremely important for practical applications, the material interface has been one of the most challenging subjects in computational material sciences as it combines configurational and elemental disorders. Training a force field for the solid electrolyte and lithium metal interface requires thousands of costly DFT calculations on large and complex interface structures and dozens of training iterations[38]. Here, we demonstrate the construction of the  $\text{Li}_6\text{PSCl}_5/\text{Li}$  interface model at a much lower cost using the PFD workflow. Considering the complexity of the interface, a custom base model was first constructed by fine-tuning the public DPA-2 pre-trained descriptor using 5% of the training set for the DPA-SSE model[39], a pre-trained model built specifically for sulfide electrolytes. Using this custom model as the foundation, the PFD workflow automatically generated various configurations, including interfaces,  $\text{Li}_6\text{PSCl}_5$  solid electrolyte, and metal lithium. In total, 409 labeled data points were selected for model training, and the fine-tuned model achieved rather good accuracy for such a complex system, as shown in Figure 9. After that, more than 14 thousand data points

Table III. Material systems tested using the PFD workflow. The prediction error is evaluated for the fine-tuned model.

Systems	Bulk materials		Complex materials			
	Crystal silicon	LATP solid electrolyte <sup>a</sup>	Polyisoprene chains	Amorphous $sp^3$ carbon	Doped perovskite <sup>b</sup>	Li <sub>6</sub> PSCl <sub>5</sub> /Li interface
No. of DFT data	33	138	157	655	134	409
Energy RMSE (eV/atom)	0.0019	0.0013	0.0027	0.0059	0.0010	0.0040
Force RMSE (eV/Å)	0.0389	0.0510	0.0562	0.0661	0.0472	0.0830

<sup>a</sup> Li<sub>1+x</sub>Al<sub>x</sub>Ti<sub>2-x</sub>(PO<sub>4</sub>)<sub>3</sub><sup>b</sup> Ba<sub>0.5</sub>Na<sub>0.25</sub>Bi<sub>0.25</sub>Ti<sub>0.875</sub>Zr<sub>0.125</sub>O<sub>3</sub>Figure 9. **The Li<sub>6</sub>PSCl<sub>5</sub>/Li interface model generated from PFD workflow.** The a) energy and the b) prediction error of the interphase model generated using knowledge distillation. Points with brighter color corresponds higher density. c) A snapshot of the interphase system at 5 ns.

including both bulk and interface structures were generated with the fine-tuned model in the distillation phase. The accuracy of the distilled model is very close to that of the fine-tuned model, as shown in Figure S7. This huge difference in the training set between fine-tuning and distillation addresses the great savings in computation resources by the PFD workflow. Using the distilled model, room temperature atomistic simulation of the Li<sub>6</sub>PSCl<sub>5</sub>/Li interface was carried out, revealing the rapid expansion of the disordered interface upon contact with the lithium metal, as shown in Figure 9. In summary, Table III lists the accuracy of and the number of DFT calculations used during the training of the specific force fields for all the material systems.

#### IV. DISCUSSION AND CONCLUSION

This work introduces PFD, a workflow that automatically generates material-specific force fields from a pre-trained foundation model through fine-tuning and distillation. Using the transferable knowledge of broad chemistry in the foundation model, efficient force fields for specific materials can be trained with one to two orders of magnitude fewer DFT training data, enabling the practical training of force fields for real-world materials, such as interfaces, amorphous phases, and high-entropy materials, among others. Currently, despite significant advance-

ments in universal force fields, traditional machine learning force fields, such as the standard DeePMD model, remain the preferred choice for calculating dynamic properties that require large-scale simulations, such as ionic diffusivity and thermal conductivity. This preference arises from their superior efficiency and quantitative accuracy for specific systems, which universal force fields have yet to achieve. However, traditional machine learning models typically have to be trained from scratch following a standard concurrent learning scheme, such as DPGEN, which designed to minimize costly DFT calculations but still requiring thousands of DFT data points. That is to say, neither pre-trained universal force fields nor traditional force fields have been fully utilized for material simulation at the production level. This situation would change with the introduction of PFD, when efficient force fields of real-world materials can be trained using just a few hundred DFT calculations while achieving the same first-principles accuracy by "reusing" the knowledge in the pre-trained foundation model. The PFD workflow provides a practical and automated approach to fully utilize the pre-trained model for the efficient generation of force fields. By incorporating the pre-trained model into the future standard of force field training, PFD enables accurate, high-throughput simulations of important material properties which are previously intractable due to difficult force field training, and hence may have significant implication in computational material sciences.

While the current PFD workflow offers significant benefits, there remain several further improvements in the design of the PFD workflow. Exploration methods beyond molecular dynamics can be integrated, providing alternative options in sampling the potential energy surface of complex materials. For instance, amorphous phases are gaining importance in fields such as solid-state electrolytes, but molecular dynamics exploration is inefficient for these materials because of the presence of many degenerate, metastable states. In addition to material simulations, the PFD can also be coupled with structure exploration algorithms such as CALYPSO[40, 41]. With the iterative "on-the-fly" fine-tuning scheme, stable structures can be rapidly filtered out from initial-guess structures with better reliability than simply using pre-trained universal force fields.

It should be noted that, in principle, the PFD framework can be applied to any pre-trained foundation model, not just the pre-trained DPA-2 used in this work. With the rapid development of pre-trained large atomic models, we are optimistic about the prospect of the PFD when future generations of foundation models with better accuracy and generalizability can be incorporated. In addition, the training target for PFD is not limited to energy and force prediction. Principally, any material properties that are dependent on material structures can be fitted to atomic descriptors by a deep learning network. If the descriptor is initially pre-trained on tasks such as energy prediction, then it can be fine-tuned with minimal training data to create a prediction model for a different, but *related* task. For example, a model predicting the experimental electronic energy gap can be fine-tuned based

on the atomic representation of a pre-trained force field model. This strategy is valuable because the experimental data is usually extremely expensive and sparse. We expect the PFD paradigm will find widespread applications in materials science for both computational simulations and direct property predictions.

## V. CODE AVAILABILITY

The source code of PFD is implemented at <https://github.com/ruoyuwang1995nya/pfd-kit>.

## SUPPLEMENTARY MATERIALS

Supplementary materials are available at repository <https://github.com/ruoyuwang1995nya/pfd-paper.git>.

## ACKNOWLEDGMENTS

This work was supported by the National Key R&D Program of China (Grants No. 2021YFA0718900 and No. 2022YFA1403000), Key Research Program of Frontier Sciences of CAS (Grant No. ZDBS-LY-SLH008), National Nature Science Foundation of China (Grants No. 12374096 and No. 92477114). We thank Zicheng Wang for providing additional test dataset. We thank Dr. Mengchao Shi of DP Technology for valuable discussion on PFD workflow. We also appreciate DP Technology for supporting with computational resource via Bohrium online platform.

- 
- [1] L. Zhang, J. Han, H. Wang, R. Car, and W. E, Physical Review Letters **120**, 143001 (2018).
- [2] A. P. Bartók, M. C. Payne, R. Kondor, and G. Csányi, Physical Review Letters **104**, 136403 (2010).
- [3] F. Noé, A. Tkatchenko, K.-R. Müller, and C. Clementi, Annual Review of Physical Chemistry **71**, 361 (2020).
- [4] H. Wang, T. Fu, Y. Du, W. Gao, K. Huang, Z. Liu, P. Chandak, S. Liu, P. Van Katwyk, A. Deac, A. Anandkumar, K. Bergen, C. P. Gomes, S. Ho, P. Kohli, J. Lasenby, J. Leskovec, T.-Y. Liu, A. Manrai, D. Marks, B. Ramsundar, L. Song, J. Sun, J. Tang, P. Veličković, M. Welling, L. Zhang, C. W. Coley, Y. Bengio, and M. Zitnik, Nature **620**, 47 (2023).
- [5] K. T. Schütt, H. E. Sauceda, P.-J. Kindermans, A. Tkatchenko, and K.-R. Müller, The Journal of Chemical Physics **148**, 241722 (2018).
- [6] L. Zhang, H. Wang, R. Car, and W. E, Physical Review Letters **126**, 236001 (2021).
- [7] J. Behler and M. Parrinello, Physical Review Letters **98**, 146401 (2007).
- [8] A. P. Bartók, J. Kermode, N. Bernstein, and G. Csányi, Physical Review X **8**, 041048 (2018).
- [9] L. Zhang, D.-Y. Lin, H. Wang, R. Car, and W. E, Physical Review Materials **3**, 023804 (2019).
- [10] T. Kostiuchenko, F. Körmann, J. Neugebauer, and A. Shapeev, npj Computational Materials **5**, 55 (2019).
- [11] V. L. Deringer, N. Bernstein, A. P. Bartók, M. J. Cliffe, R. N. Kerber, L. E. Marbella, C. P. Grey, S. R. Elliott, and G. Csányi, The Journal of Physical Chemistry Letters **9**, 2879 (2018).
- [12] D. Zhang, X. Liu, X. Zhang, C. Zhang, C. Cai, H. Bi, Y. Du, X. Qin, A. Peng, J. Huang, B. Li, Y. Shan, J. Zeng, Y. Zhang, S. Liu, Y. Li, J. Chang, X. Wang, S. Zhou, J. Liu, X. Luo, Z. Wang, W. Jiang, J. Wu, Y. Yang, J. Yang, M. Yang, F.-Q. Gong, L. Zhang, M. Shi, F.-Z. Dai, D. M. York, S. Liu, T. Zhu, Z. Zhong, J. Lv, J. Cheng, W. Jia, M. Chen, G. Ke, W. E, L. Zhang, and H. Wang, npj Computational Materials **10**, 293 (2024).
- [13] H. Yang, C. Hu, Y. Zhou, X. Liu, Y. Shi, J. Li, G. Li, Z. Chen, S. Chen, C. Zeni, M. Horton, R. Pinsler, A. Fowler, D. Zügner, T. Xie, J. Smith, L. Sun, Q. Wang, L. Kong, C. Liu, H. Hao, and Z. Lu, "MatterSim: A Deep Learning Atomistic Model Across Elements, Temperatures and Pressures," (2024), arXiv:2405.04967 [cond-



- mat].
- [14] M. Neumann, J. Gin, B. Rhodes, S. Bennett, Z. Li, H. Choubisa, A. Hussey, and J. Godwin, “Orb: A Fast, Scalable Neural Network Potential,” (2024), arXiv:2410.22570 [cond-mat].
- [15] I. Batatia, D. P. Kovács, G. N. C. Simm, C. Ortner, and G. Csányi, “MACE: Higher Order Equivariant Message Passing Neural Networks for Fast and Accurate Force Fields,” (2023), arXiv:2206.07697 [cond-mat, physics:physics, stat].
- [16] I. Batatia, P. Benner, Y. Chiang, A. M. Elena, D. P. Kovács, J. Riebesell, X. R. Advincula, M. Asta, M. Avaylon, W. J. Baldwin, F. Berger, N. Bernstein, A. Bhowmik, S. M. Blau, V. Cărare, J. P. Darby, S. De, F. D. Pia, V. L. Deringer, R. Elijošius, Z. El-Machachi, F. Falcioni, E. Fako, A. C. Ferrari, A. Genreith-Schriever, J. George, R. E. A. Goodall, C. P. Grey, P. Grigorev, S. Han, W. Handley, H. H. Heenen, K. Hermansson, C. Holm, J. Jaafar, S. Hofmann, K. S. Jakob, H. Jung, V. Kapil, A. D. Kaplan, N. Karimitari, J. R. Kermode, N. Kroupa, J. Kullgren, M. C. Kuner, D. Kuryla, G. Liepuoniute, J. T. Margraf, I.-B. Magdău, A. Michaelides, J. H. Moore, A. A. Naik, S. P. Niblett, S. W. Norwood, N. O’Neill, C. Ortner, K. A. Persson, K. Reuter, A. S. Rosen, L. L. Schaaf, C. Schran, B. X. Shi, E. Sivonxay, T. K. Stenczel, V. Svahn, C. Sutton, T. D. Swinburne, J. Tilly, C. v. d. Oord, E. Varga-Umbrich, T. Vegge, M. Vondrák, Y. Wang, W. C. Witt, F. Zills, and G. Csányi, “A foundation model for atomistic materials chemistry,” (2024), arXiv:2401.00096 [physics].
- [17] C. Chen and S. P. Ong, *Nature Computational Science* **2**, 718 (2022).
- [18] F. Xie, T. Lu, S. Meng, and M. Liu, *Science Bulletin* **69**, 3525 (2024).
- [19] B. Deng, P. Zhong, K. Jun, J. Riebesell, K. Han, C. J. Bartel, and G. Ceder, *Nature Machine Intelligence* **5**, 1031 (2023).
- [20] L. Barroso-Luque, M. Shuaibi, X. Fu, B. M. Wood, M. Dzamba, M. Gao, A. Rizvi, C. L. Zitnick, and Z. W. Ulissi, “Open Materials 2024 (OMat24) Inorganic Materials Dataset and Models,” (2024), arXiv:2410.12771 [cond-mat].
- [21] S. Takamoto, C. Shinagawa, D. Motoki, K. Nakago, W. Li, I. Kurata, T. Watanabe, Y. Yayama, H. Iriguchi, Y. Asano, T. Onodera, T. Ishii, T. Kudo, H. Ono, R. Sawada, R. Ishitani, M. Ong, T. Yamaguchi, T. Kataoka, A. Hayashi, N. Charoenphakdee, and T. Ibuka, *Nature Communications* **13**, 2991 (2022).
- [22] Y.-L. Liao, B. Wood, A. Das, and T. Smidt, “EquiformerV2: Improved Equivariant Transformer for Scaling to Higher-Degree Representations,” (2024), arXiv:2306.12059 [cs].
- [23] M. Geiger and T. Smidt, “e3nn: Euclidean Neural Networks,” (2022), arXiv:2207.09453 [cs].
- [24] A. Merchant, S. Batzner, S. S. Schoenholz, M. Aykol, G. Cheon, and E. D. Cubuk, *Nature* (2023), 10.1038/s41586-023-06735-9.
- [25] J. Zeng, D. Zhang, D. Lu, P. Mo, Z. Li, Y. Chen, M. Rynik, L. Huang, Z. Li, S. Shi, Y. Wang, H. Ye, P. Tuo, J. Yang, Y. Ding, Y. Li, D. Tisi, Q. Zeng, H. Bao, Y. Xia, J. Huang, K. Muraoka, Y. Wang, J. Chang, F. Yuan, S. L. Bore, C. Cai, Y. Lin, B. Wang, J. Xu, J.-X. Zhu, C. Luo, Y. Zhang, R. E. A. Goodall, W. Liang, A. K. Singh, S. Yao, J. Zhang, R. Wentzcovitch, J. Han, J. Liu, W. Jia, D. M. York, W. E. R. Car, L. Zhang, and H. Wang, *The Journal of Chemical Physics* **159**, 054801 (2023).
- [26] X. Liu, Y. Han, Z. Li, J. Fan, C. Zhang, J. Zeng, Y. Shan, Y. Yuan, W.-H. Xu, Y.-P. Liu, Y. Zhang, T. Wen, D. M. York, Z. Zhong, H. Zheng, J. Cheng, L. Zhang, and H. Wang, “Dflow, a Python framework for constructing cloud-native AI-for-Science workflows,” (2024), arXiv:2404.18392 [cs].
- [27] H.-J. Deiseroth, S.-T. Kong, H. Eckert, J. Vannahme, C. Reimer, T. Zaiß, and M. Schlosser, *Angewandte Chemie* **120**, 767 (2008), publisher: WILEY-VCH Verlag Weinheim.
- [28] Y. Zhang, H. Wang, W. Chen, J. Zeng, L. Zhang, H. Wang, and W. E, *Computer Physics Communications* **253**, 107206 (2020).
- [29] A. Rossbach, F. Tietz, and S. Grieshammer, *Journal of Power Sources* **391**, 1 (2018).
- [30] T. Famprakis, P. Canepa, J. A. Dawson, M. S. Islam, and C. Masquelier, *Nature Materials* **18**, 1278 (2019).
- [31] A. Van der Ven, Z. Deng, S. Banerjee, and S. P. Ong, *Chemical Reviews* **120**, 6977 (2020).
- [32] X. He, Y. Zhu, and Y. Mo, *Nature Communications* **8**, 15893 (2017).
- [33] V. L. Deringer and G. Csányi, *Physical Review B* **95**, 094203 (2017).
- [34] X. Shi, C. He, C. J. Pickard, C. Tang, and J. Zhong, *Physical Review B* **97**, 014104 (2018).
- [35] Y. Shi, R. He, B. Zhang, and Z. Zhong, .
- [36] J. Wu, J. Yang, Y.-J. Liu, D. Zhang, Y. Yang, Y. Zhang, L. Zhang, and S. Liu, *Physical Review B* **108**, L180104 (2023).
- [37] Y. Xiao, Y. Wang, S.-H. Bo, J. C. Kim, L. J. Miara, and G. Ceder, *Nature Reviews Materials* **5**, 105 (2019).
- [38] Y. An, T. Hu, Q. Pang, and S. Xu, “Observing li nucleation at li metal-solid electrolyte interface in all-solid-state batteries,” (2024), arXiv: 2412.12611 [cond-mat.mtrl-sci].
- [39] R. Wang, M. Guo, Y. Gao, X. Wang, Y. Zhang, B. Deng, X. Chen, M. Shi, L. Zhang, and Z. Zhong, “A Pre-trained Deep Potential Model for Sulfide Solid Electrolytes with Broad Coverage and High Accuracy,” (2024), arXiv:2406.18263 [physics].
- [40] Y. Wang, J. Lv, L. Zhu, and Y. Ma, *Computer Physics Communications* **183**, 2063 (2012).
- [41] Y. Wang, J. Lv, L. Zhu, and Y. Ma, *Physical Review B* **82**, 094116 (2010).